JOURNAL OF CATALYSIS 125, 353–375 (1990)

Structure and Composition Requirements for Deoxygenation, Dehydration, and Ketonization Reactions of Carboxylic Acids on TiO_2(001) Single-Crystal Surfaces

K. S. KIM[1] AND M. A. BARTEAU[2]

Center for Catalytic Science and Technology, Department of Chemical Engineering, University of Delaware, Newark, Delaware 19716

Received November 27, 1989; revised April 2, 1990

The reactivities of TiO_2(001) single-crystal surfaces for acetic acid decomposition were studied by TPD and XPS. Surface structure and composition were varied by a combination of argon ion bombardment and annealing in order to investigate reaction selectivity and to identify the active sites responsible for adsorption and decomposition. Acetic acid adsorbed both molecularly and dissociatively at 200 K, but only dissociatively at 300 K. The molecular species desorbed readily below 300 K. Approximately 15% of the dissociatively adsorbed species (acetates) desorbed as acetic acid at 390 K via recombination with surface hydroxyls. The remaining acetates decomposed at higher temperatures via three different reaction pathways with selectivities dependent on surface composition and structure. Reduced surfaces containing Ti cations of lower valences favored direct deoxygenation of the acetates to fill the oxygen vacancies of the surface. This reaction occurred even at room temperature and deposited atomic carbon on the surface. Oxidized surfaces containing only Ti^{4+} cations favored reactions to form volatile molecular products. On the {011}-faceted surface, surface acetates decomposed via net unimolecular dehydration to ketene. On the {114}-faceted surface, the bimolecular reaction of surface acetates to form acetone also took place. The reactions of propionates formed by dissociation of propionic acid were directly analogous to those of acetates: methyl ketene was produced by net unimolecular dehydration on the {011}-faceted surface and 3-pentanone was the bimolecular ketonization product on the {114}-faceted surface. Since the {011}-faceted surface exposes only Ti^{4+} cations of fivefold oxygen coordination, these sites were determined to be responsible for the net unimolecular dehydration. Bimolecular ketonization required the coordination of two acetates to a common Ti^{4+} cation on a stoichiometric surface. Of the single-crystal surfaces examined, only the {114}-faceted surface presented the necessary fourfold oxygen-coordinated Ti^{4+} sites for this reaction.

INTRODUCTION

The concept of structure sensitivity is well established for reactions catalyzed by metals. Examples of structure-sensitive reactions have generally been demonstrated by the use of supported metal catalysts exhibiting different particle sizes. As pointed out by Boudart and Djega-Mariadassou (*1*), these studies and the concept of structure sensitivity itself have received important confirmation from experiments with macroscopic metal single crystals on which different surface structures have been produced. Even with this connection to single-crystal studies, the site requirements for structure-sensitive reactions on metals are often defined in terms of the size of the ensemble of metal atoms, rather than specific crystallographic structures.

The concept of structure sensitivity in catalysis by metal oxides is considerably less well developed than in catalysis by metals, in spite of the growing number of examples of such reactions (*2*). There are several rea-

[1] Present address: Catalyst Research Laboratory, Ulsan Research Center, Yukong Ltd., P.O. Box 4, Ulsan, Kyung-Nam, South Korea.

[2] To whom correspondence should be addressed.

0021-9517/90 $3.00

sons for this evolutionary difference. First, as recently noted (*3*) the linkage between structure sensitivity and specificity to a given metal does not appear to be as generally applicable to oxides as to metals. Dissociation of acids occurs on many oxides, but may still require specific crystallographic planes on any given oxide. Second, at the same time that the expectations for definition of specific site structures have been higher on oxides than on metals, the tactics for realizing these have been more limited. The most common route for examining structure sensitivity in catalysis by oxides has involved the variation of crystallite morphologies, often by use of novel preparation methods. Characterization of oxide catalysts is generally more problematical than that of metals; it is difficult, for example, to titrate the active surface areas of supported oxides by chemisorption techniques.

Studies of the relationship between the crystallite morphology of single-component oxides and the activity and selectivity of these materials have provided much of the basis for attributing catalytic behavior to specific crystallographic planes. However, there exists considerable disagreement among such studies in the literature. For example, Sleight and co-workers (*4, 5*) have provided evidence that the (010) basal plane of orthorhombic α-MoO_3 is inactive for adsorption or oxidation of methanol; Tatibouet *et al.* (*6, 7*) contend that formaldehyde is produced on the (010) face as well as on the apical (001) and (101) faces. Side products such as methylal and dimethyl ether are also attributed to the apical planes by the latter group. A similar discrepancy exists in the interpretation of propylene oxidation on this oxide (*8*). Volta *et al.* (*2, 9, 10*) have reported that selective oxidation to acrolein occurs on the apical faces with unselective combustion on the basal plane; Haber and co-workers (*11*) have concluded that acrolein formation occurs on the basal plane. This situation is not unique to MoO_3. Bowker *et al.* (*12*) have determined that dissociation of alcohols occurs only on the polar surfaces of zinc oxide, whereas Djega-Mariadassou *et al.* (*13*) concluded that such reactions are structure insensitive. A portion of this confusion appears to have arisen from attempts to establish structure-selectivity relations for reactions in which selectivity is a strong function of conversion (e.g., as in sequential oxidation steps) or in which there is significant inhibition by the reaction products. Structure–activity relationships produced by variation of crystallite morphology appear to be somewhat less ambiguous, although this approach offers no way to distinguish the properties of crystallographic planes whose population varies in tandem (e.g., the two polar planes of zinc oxide).

Studies of the reactivity of macroscopic oxide single crystals hold the promise of resolving such dilemmas, yet for a variety of reasons the surface science of oxides is considerably less well developed than that of metals. This situation is changing rapidly; recent studies from this laboratory (*3, 14–17*) and from others (*18, 19*) have established that dissociation of Brønsted acids, including alcohols, occurs exclusively on the (0001)-Zn polar plane of ZnO.

Among the many difficulties in performing surface science studies of oxide crystals is the greater tendency than one typically encounters with metals of low-index planes of oxides to undergo thermal faceting. The desire for simplicity typically leads to the avoidance of such surfaces and therefore to the choice of oxide surfaces with the greatest average coordination number, as these tend to exhibit greater stability. However, provided that the structures of the faceted surfaces are sufficiently well resolved, one can exploit this behavior to examine the variation of activity and selectivity with progressive changes in structure of a single surface. We report here such a study of the reactions of acetic and propionic acids on faceted TiO_2(001) surfaces.

In the present study, experiments were conducted in ultrahigh-vacuum environments with TiO_2(001) single-crystal sur-

faces. Surface structure and composition were varied by the combination of argon ion bombardment and annealing and were characterized by low energy electron diffraction (LEED) and Auger electron spectroscopy (AES). The reactivity of each surface was investigated by means of temperature-programmed desorption (TPD) and X-ray photoelectron spectroscopy (XPS). The results of this study demonstrate that experiments on single-crystal oxide surfaces using surface science techniques can resolve the roles of surface structure and composition in catalytic reactions on metal oxides.

EXPERIMENTAL

Experiments were performed in two different UHV systems which have been described previously in detail (*14, 21*). TPD experiments were conducted in a Physical Electronics Model 548 surface analysis system with AES and LEED capability, equipped with a UTI 100C quadrupole mass spectrometer, and XPS experiments were conducted in a PHI Model 550 ESCA/AES surface analysis system. Typical base pressures in both vacuum chambers were 2×10^{-10} Torr. The TiO_2 single crystal ($10 \times 9 \times 1.5$ mm) used in this study was prepared from a rutile crystal boule (99.9%, Atomergic Chemetals Corp.) aligned to within $\pm 0.5°$ of the (001) orientation by Laue method. The crystal mounting and cleaning procedures were identical to those used previously (*22*). Ion bombardment and subsequent annealing of the sample produced slight reduction of the bulk, resulting in an electrically conductive oxide sample. As shown below, annealing reoxidized the surface by diffusion of oxygen from the sample bulk. For the clean, fully annealed crystal, the ratio of the peak-to-peak height of the O(KLL) Auger transition at 510 eV to that of the Ti(LMM) transition at 380 eV was ca. 1.65–1.70. This ratio, the annealing conditions required to produce it, and the corresponding Ti(2*p*) XPS spectra were characteristic of a fully oxidized TiO_2 surface (*23*) as shown below. All Auger measurements were conducted by using a 2-keV electron beam at 2 mA emission current. The electron beam was defocused on the crystal at a sample current of 0.1 μA in order to avoid surface reduction caused by electron beam damage. The details of preparation of each surface precede the results obtained from each below.

A typical TPD experiment consisted of initially dosing the crystal at the desired temperature with the reactant. After dosing, the crystal was positioned in front of the mass spectrometer and the chamber was allowed to pump down until a stable background pressure, typically 1×10^{-9} Torr, was reached. Heating was then initiated and the desorption flux was monitored by the mass spectrometer which was multiplexed with an IBM personal computer. As many as eight masses were scanned simultaneously as a function of temperature during a single TPD experiment. The computer was also used to control the heating rate of the crystal. A heating rate of 1.2 K/s was used in TPD experiments. In order to minimize contributions to the desorption spectra from species adsorbed on the sample-mounting hardware, the ionizer of the mass spectrometer probe was enclosed by a cylindrical quartz envelope with a small aperture at the end. The procedures for identification and quantitative analysis of reaction products (including higher molecular weight coupling products) have been described in detail in our previous studies of the reactions of alcohols and carboxylic acids on TiO_2 single crystals and powders (*20, 22, 24*). In brief, these consisted of the following steps: (i) integration of the peak areas for all mass fragments monitored, (ii) subtraction of the contributions from desorption of the reactant, (iii) assignment of peaks to reaction products in accord with experimentally determined fragmentation patterns, and (iv) calculation of quantitative distributions by use of sensitivity factors calculated by the method of Ko *et al.* (*25*).

A typical XPS experiment consisted of an

initial exposure of the crystal using the same procedure as that for the TPD experiments. The crystal was then positioned under the Al X-ray source and the spectra were collected. During XPS data collection, the Ti($2p_{1/2,3/2}$), O(1*s*), and C(1*s*) regions were scanned over a 30-min period for each set of spectra, with the X-ray source operated at an emission current of 60 mA and a 10 keV accelerating voltage. For experiments in which XPS spectra were collected as a function of temperature, the first set of spectra in the series was collected as described above; for subsequent sets of spectra the crystal was first heated to the desired temperature, held at that temperature briefly (less than 5 s), and then allowed to cool to the original dosing temperature before spectra were collected. The same heating rate as that used in TPD experiments was used during the intermittent heating sequences in XPS experiments.

CH_3COOH (Fisher Scientific, 99.7%), CH_3COOD (Chemical Dynamics, 99.5%), and C_2H_5COOH (Aldrich, 99 + %) were contained in glass sample tubes attached to the dosing manifold. These reactants were purified by repeated freeze–pump–thaw cycles prior to use. The reactant vapors were dosed onto the crystal through variable leak valves equipped with stainless-steel dosing needles. Dosing was conducted both with the TiO_2 crystal at room temperature and at low temperatures; the lowest temperatures achieved were 165 K for XPS experiments and 200 K for TPD experiments. For each reactant, the dosing manifold pressure, dosing time, and number of dosing cycles were varied until the saturation exposure was reached. The dosing manifold pressure was maintained below 100 μm in order to minimize the formation of carboxylic acid dimers. At room temperature, the equilibrium dimer mole fraction at this pressure is less than 10% (*26*). Experiments at line pressures up to 1000 μm showed no differences; indeed we have found no evidence for distinguishable reactions of dimers adsorbed from the gas phase in any study of carboxylic acids on metals or metal oxides from this laboratory (*16, 26*). All TPD and XPS data reported in this study were obtained for saturation exposures. For acetic acid, TPD and XPS experiments were carried out on the Ar^+-bombarded surface and on surfaces annealed at several different temperatures between 500 and 950 K after the Ar^+-bombardment. For propionic acid, only the 750 K annealed and 950 K annealed surfaces were investigated.

RESULTS

1. Carbon-Covered Surface

Before collecting the data for the clean surfaces, TPD experiments were conducted on an unsputtered, carbon-covered TiO_2(001) surface. The Auger C(270 eV)/Ti(380 eV) peak-to-peak ratio for this surface was greater than 0.5, indicating that the single-crystal surface was substantially covered with carbon. Following CH_3COOH adsorption at 300 K, species such as CH_3COOH, CO, and CO_2 were observed upon heating. CH_3COOH exhibited a small desorption peak at 390 K. This peak most likely resulted from molecularly adsorbed acetic acid since surface carbon would be expected to suppress dissociative adsorption. CO and CO_2 exhibited small peaks around 425 K attributed to CH_3COOH decomposition on the sample-mounting hardware due to their low peak temperatures. These peaks were also observed in the TPD spectra obtained on the initially clean surfaces; they have been omitted from the TPD results reported for the clean surfaces as they appeared to represent desorption from surfaces other than that of the TiO_2 single crystal. The CO desorption signal from the carbon-covered surface began to increase rapidly around 550 K. This resulted from the burn-off of surface carbon, since this phenomenon was also observed in a blank TPD experiment on the carbon-covered surface, while a blank TPD experiment on the clean surface exhibited a flat CO desorption signal. H_2O did not exhibit a distinct desorption peak but rather increased gradually. Es-

sentially identical results were obtained in TPD of C_2H_5COOH on the carbon-covered surface. The absence of significant reaction of acetic acid (or propionic acid) in experiments with a carbon-covered surface demonstrated that contributions to the TPD spectra from adsorption and decomposition on the sample-mounting hardware were effectively eliminated by enclosing the mass spectrometer ionizer.

2. *Clean Surfaces*

2.1 Surface Preparation

TiO_2(001) surfaces with different structures and compositions were prepared by controlling the annealing temperature subsequent to Ar^+ bombardment. Annealing was conducted in vacuum for periods of 20 min at temperatures from 400 to 950 K. A highly reduced, disordered surface was produced by sputtering the clean, fully oxidized surface with a 2-keV Ar^+ beam for 1 h. The Auger O/Ti peak-height ratio was ca. 1.20, typical of an oxygen-deficient TiO_2 surface (*23*). No LEED pattern was observed for this surface. The Ti(2*p*) XPS spectrum obtained for this surface was broad and poorly resolved, as shown by curve (a) in Fig. 1, characteristic of a partially reduced TiO_2 surface. This spectrum could be fit by three ($2p_{1/2,3/2}$) doublets at 465.0/459.3 eV (Ti^{4+}), 463.2/457.6 eV (Ti^{3+}), and 461.1/455.5 eV (Ti^{2+}) (*27*), consistent with the presence of Ti_2O_3 and TiO. Annealing the sputtered single crystal at 400, 500, and 600 K did not result in significant oxidation or ordering of the surface, as evidenced by the absence of notable changes in the AES, LEED, and XPS data. Annealing at 650 K increased the extent of surface oxidation and ordering; the AES O/Ti ratio increased to 1.37 and a rather indistinct LEED pattern was observed. The Ti(2*p*) XPS spectrum obtained for this surface (curve (b), Fig. 1) resembled that reported for a stoichiometric Ti_2O_3 surface (*28*). The extent of surface oxidation and ordering was further increased by annealing at 700 K, as evidenced by the AES

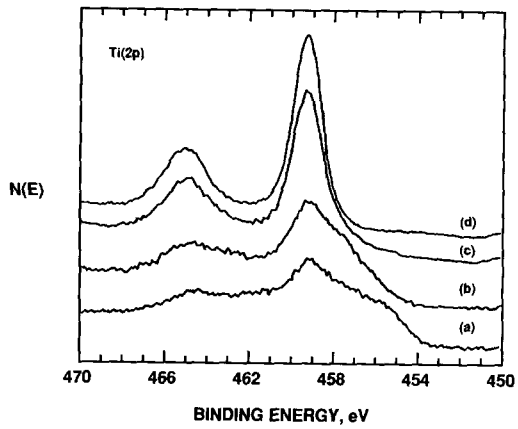

FIG. 1. Ti(2*p*) XPS spectra of the TiO_2(001) surface as a function of annealing temperature. The Ar^+-bombarded (001) single crystal was annealed for 20 min at progressively increasing temperatures: (a) sputtered, (b) 650 K, (c) 700 K, (d) 750, 800, 850, and 950 K.

O/Ti ratio of 1.42 and the sharper LEED pattern observed for the 700 K-annealed surface. The Ti(2*p*) XPS spectrum obtained for this surface, curve (c) in Fig. 1, demonstrated that the surface consisted of nearly stoichiometric TiO_2 together with very small amounts of suboxide, probably Ti_2O_3.

The Ar^+-bombarded surface was transformed into an oxidized, {011}-faceted surface by annealing at 750 K. A sharp LEED pattern, which was in good agreement with that referred to as the "low-temperature phase" and assigned to the (2 × 1) reconstructed {011}-faceted structure by Firment (*29*), was observed for this surface. The AES O/Ti peak-height ratio increased to 1.48, indicative of surface oxidation in the course of annealing. The Ti(2*p*) XPS spectrum obtained for the {011}-faceted surface exhibited well-resolved Ti($2p_{1/2}$) and Ti($2p_{3/2}$) peaks at 465.0 and 459.3 eV, respectively, as displayed by curve (d) in Fig. 1. These binding energies, together with the full-width-at-half-maximum (FWHM) of the Ti($2p_{3/2}$) peak, 1.65 eV, are characteristic of Ti^{4+} species in TiO_2 (*23*). The Ti cations of the {011}-faceted surface are exclusively fivefold oxygen-coordinated (*29, 30*). Annealing at temperatures higher than 750 K

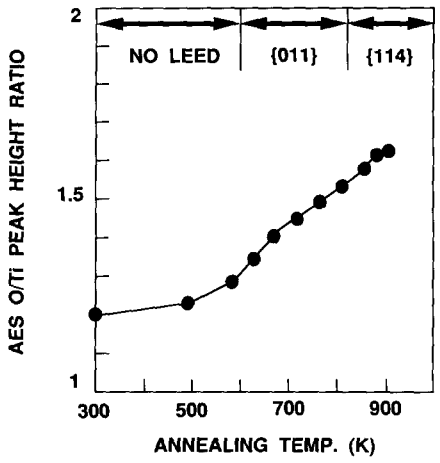

FIG. 2. Auger O/Ti peak-height ratio and LEED pattern index of the Ar^+-bombarded $TiO_2(001)$ single crystal as a function of annealing temperature.

brought about further oxidation and faceting of the surface, as evidenced by the progressive increase in the AES O/Ti ratio and the appearance of additional diffraction spots in the LEED pattern. Annealing at 950 K produced a more completely oxidized, {114}-faceted surface. The LEED pattern for this surface resembled closely that designated as the "high-temperature phase" by Firment (*29*). The AES O/Ti peak-height ratio for the high-temperature phase was 1.66, in good agreement with those reported for the TiO_2 single-crystal surfaces completely oxidized under vacuum (*23*). However, the Ti(2*p*) and O(1*s*) spectra obtained from this surface exhibited no changes compared to the 750 K-annealed, {011}-faceted surface. The {114}-faceted surface is a stepped structure with Ti^{4+} cations of four-, five-, and sixfold oxygen-coordination (*29, 30*). In Fig. 2 is presented the variation of the AES O/Ti peak-height ratio and LEED pattern of the Ar^+-bombarded $TiO_2(001)$ single-crystal surface as a function of annealing temperature. Figure 3 illustrates the structures of the {011}- and {114}-faceted $TiO_2(001)$ surfaces proposed by Firment (*29*); these provide the basis for our determination of structure–reactivity relationships for this material.

2.2 CH_3COOH Decomposition

2.2.1 Reduced surfaces. It was shown above that for annealing treatments at temperatures below 750 K the Ar^+-bombarded $TiO_2(001)$ single-crystal surface remained oxygen-deficient. The reactivities of these reduced surfaces were investigated by TPD and XPS for CH_3COOH decomposition. First, data for the Ar^+-bombarded surface are reported.

A set of TPD spectra following adsorption of CH_3COOH at 300 K on a sputtered, unannealed TiO_2 surface is displayed in Fig. 4. Two desorption states were evidenced by two groups of desorption peaks at different temperatures. The peak temperatures were consistent with those observed on polycrystalline anatase powders (*20*). The lower temperature group included CH_3COOH and H_2O peaks coincident at 390 K. The higher temperature group consisted of an additional CH_3COOH peak at 585 K, CO and CH_4 peaks at 600 K, a CH_2CO (ketene) peak at 610 K, and an additional H_2O peak at 650 K. H_2 desorption appeared as a very weak peak around 600 K imposed on a

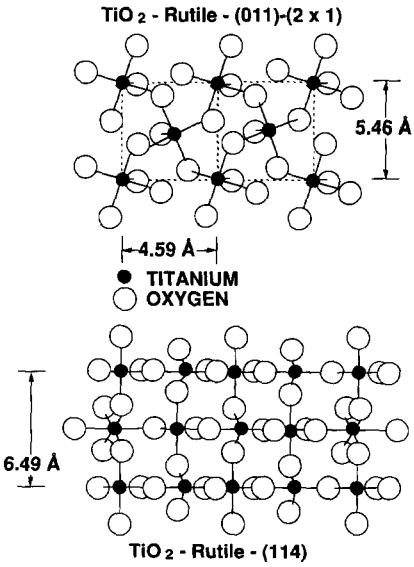

FIG. 3. Depiction of the structures of the {011} and {114}-faceted $TiO_2(001)$ surfaces, revised and redrawn from Firment (*29*).

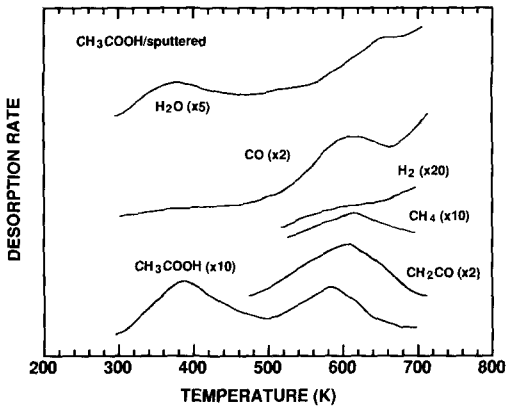

FIG. 4. TPD spectra following CH_3COOH adsorption at 300 K on the Ar^+-bombarded TiO_2(001) surface. The spectra are uncorrected for mass spectrometer sensitivities and are offset for distinction.

slowly rising signal. The amounts of CH_3COOH desorbed at 390 and 585 K were comparable. The amount of CH_2CO desorption was four times that of the CH_3COOH desorbed at 585 K. In the case of CO desorption, the signal increased very rapidly above 650 K; thus quantitative determination of the desorption yield was difficult. Similar behavior was also observed for the high temperature H_2O desorption. Other molecules which were checked for but not detected included CO_2, $(CH_3)_2CO$, C_2H_4, C_2H_6, CH_3CHO, and $HCOOCH_3$. The relative product yields for volatile products from CH_3COOH TPD on the Ar^+-bombarded TiO_2(001) single crystal are listed in Table 1. Since these experiments resulted in the deposition of significant coverages of atomic carbon on the surface, computation of the fraction of adsorbed acetic acid converted to each product required additional information from XPS experiments, as shown below.

In order to investigate the importance of desorption from the ceramic adhesive used for thermocouple attachment, a separate series to TPD experiments was carried out with a press-fit of the thermocouple onto the crystal surface using a tantalum clip. These experiments obtained the same product distribution as that listed in Table 1; thus no contribution from the ceramic adhesive was evident. However, when the thermocouple was in contact with the tantalum clip the peak temperatures shifted upward in a nonlinear fashion due to the temperature gradient between the crystal surface and the clip. For example, the CH_3COOH peak at 390 K and the CH_2CO peak at 610 K shifted to 560 and 965 K, respectively. These shifts demonstrated the importance of reliable measurement of metal oxide surface temperatures (*14, 22, 31*).

The surface intermediates formed during CH_3COOH decomposition on the Ar^+-bombarded TiO_2(001) surface were identified and their populations tracked by XPS. During XPS experiments, the Ti($2p_{3/2}$) peak was found to shift to lower binding energy as reactants were dosed onto the surface. In order to facilitate comparison, individual spectra were referenced to the binding energy of the Ti($2p_{3/2}$) peak for Ti^{4+} in TiO_2, fixed at 459.3 eV. A typical set of C(1*s*) spectra for the CH_3COOH-dosed surface as a function of surface temperature is displayed in Fig. 5. Following CH_3COOH adsorption at 300 K, two C(1*s*) peaks centered at 289.6 and 285.8 eV were observed, as shown in curve (a). The FWHM of each C(1*s*) peak was 1.8 eV. The C(1*s*) peak at 289.6 eV was assigned to the carboxyl carbon and the peak at 285.8 eV to the methyl group carbon. The C(1*s*) peak positions and

TABLE 1

Relative Product Yields for CH_3COOH TPD on the Ar^+-Bombarded TiO_2(001) Surface

Product	Peak temp (K)	Relative yield	Molar yield per mole CH_3COOH adsorbed
CH_3COOH	390	0.31	0.09
H_2O	390	0.07	0.02
CH_3COOH	585	0.24	0.07
CO	600	Not quantified	1.1[a]
CH_4	600	0.04	0.01
CH_2CO	610	1.00	0.28
H_2O	650	Not quantified	

[a] The CO yield was calculated from the overall carbon balance (see text).

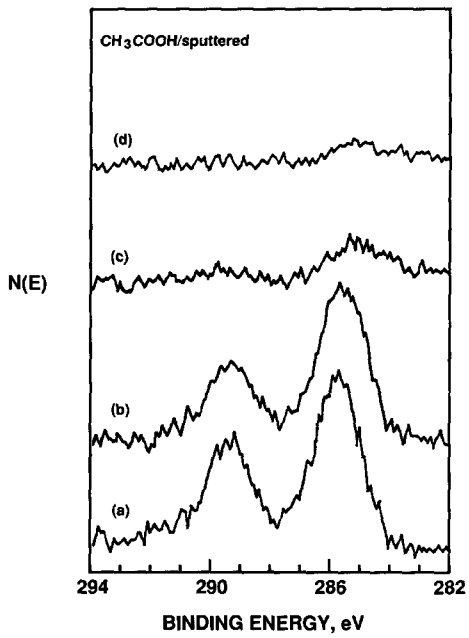

FIG. 5. C(1*s*) XPS spectra for CH_3COOH adsorbed on the Ar^+-bombarded TiO_2(001) surface as a function of surface temperature. (a) CH_3COOH-dosed surface at 300 K. (b) Surface in a heated to 425 K. (c) Surface in b heated to 600 K. (d) Surface in c heated to 650 K.

their separation were consistent with those observed for adsorbed acetate species on oxidized TiO_2 surfaces in this study. The ratio of the area of the carboxyl carbon peak to the area of the methyl carbon peak was 0.7. This ratio was somewhat smaller than the value, 0.85, observed for adsorbed acetate species on the oxidized TiO_2 surfaces. This indicates that the surface intermediates formed at 300 K on the sputtered TiO_2 surface consisted of more than one species derived from CH_3COOH. These intermediates are likely to be adsorbed acetate species and adsorbed hydrocarbon fragments. It can be deduced that some portion of the adsorbed acetate species readily undergo decomposition at 300 K to fill the oxygen vacancies of the sputtered surface and thereby deposite hydrocarbon fragments on the surface.

Heating the CH_3COOH-dosed surface to 425 K caused the intensities of the C(1s) peaks to decrease by ca. 10% (curve (b)), indicative of the removal of adsorbates from the surface. Both C(1*s*) peaks shifted by 0.1 eV to lower binding energies. The intensity decrease is consistent with the TPD results showing a CH_3COOH peak at 390 K. Heating the surface to 500 and 550 K attenuated the C(1*s*) peaks and shifted the methyl carbon peak to progressively lower binding energies. This is consistent with the TPD results which showed that the desorption signals of CH_2CO, CH_3COOH, and CO started to increase around 470 K. Heating the surface further to 600 K resulted in significant changes in the C(1*s*) spectrum (curve (c)). The most notable change was sharp decrease in the total area of the C(1*s*) peaks. The carboxyl peak decreased nearly to the noise level, and the methyl peak shifted to 285.2 eV, very close to the binding energy of adsorbed atomic carbon. (Adsorbed atomic carbon exhibited binding energies of 284.9 ± 0.1 eV in this study.) This spectrum demonstrates that the surface intermediates at 600 K consisted of mostly atomic carbon with a very small amount of adsorbed acetate species remaining. This interpretation is consistent with the TPD results showing the desorption peaks of CH_2CO, CH_3COOH, and CO around 600 K. This series of spectra also demonstrates that those products were produced via decomposition of surface acetate species.

The carboxyl peak was removed completely by heating the surface to 650 K; however, the peak which could be assigned to atomic carbon was not removed by the same heat treatment (curve (d)). The atomic carbon peak could be completely removed only by heating the surface at 750 K for several minutes. The TPD spectrum exhibiting a rapidly rising CO signal above 650 K (displayed in Fig. 4) suggests that atomic carbon reacted to form CO via oxidation by lattice oxygen at the surface. This atomic carbon is most likely graphitic rather than carbidic on the basis of its C(1*s*) binding energy. Tanaka *et al.* (*32*) reported the C(1*s*) XPS binding energies of graphitic and carbidic carbons formed by CO_2 adsorption on TiO_2

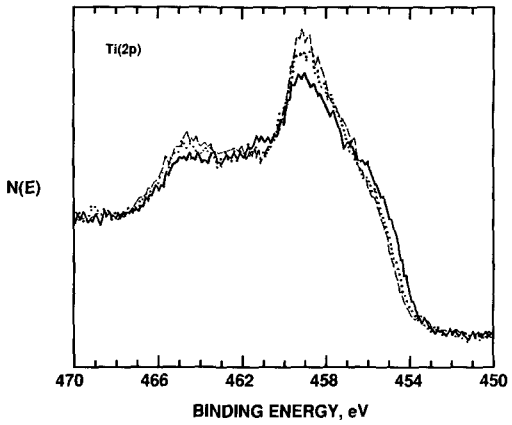

FIG. 6. Ti(2*p*) XPS spectra for the Ar^+-bombarded TiO_2(001) surface. Solid curve: clean surface at 300 K. Dotted curve: after heating the clean surface to 650 K. Dashed curve: after heating the CH_3COOH-dosed surface to 600 K.

powders. By correcting those values with reference to the Ti($2p_{3/2}$) binding energy of an oxidized surface in this study, one would expect the binding energy of graphitic carbon to be around 285.0 eV while that for carbidic carbon would be around 281.8 eV. Tanaka *et al.* observed the formation of TiC species on an Ar^+-bombarded surface. However, such species are excluded in this study on the basis of the absence of a carbidic carbon peak in the XPS spectra; the lack of carbide formation is consistent with the absence of metallic Ti on the sputtered surfaces in this study (*27*).

Ti(2*p*) spectra collected during a sequence of heat treatments showed that, when subjected to the same treatment, the CH_3COOH-dosed, Ar^+-bombarded surface became more highly oxidized than the bare, Ar^+-bombarded surface. As illustrated in Fig. 6 the CH_3COOH-dosed surface which was heated to 600 K exhibited a greater extent of surface oxidation than a bare surface which was heated to 650 K. Surface oxidation was clearly evidenced by the increase in Ti^{4+} peak intensities and the attenuation of the Ti^{2+} contribution at lower binding energies. These results demonstrate that the oxygen atoms from the adsorbates were incorporated into the surface to produce surface oxidation.

Annealing the surface to temperatures between 300 and 700 K prior to acetic acid adsorption dramatically increased the yield of organic products and reduced the yield of CO from carbon burnoff at high temperature. However, the adsorbate coverage following CH_3COOH adsorption at 300 K was quite insensitive to the prior annealing temperature as evidenced by the comparable C(1*s*) peak areas displayed in Fig. 7. Since the CO desorption peak was well resolved in TPD experiments on surfaces previously annealed at 700 K and above, and since XPS demonstrated that the initial adsorbate coverages did not change, the fractional yields of products from the reduced surfaces (for which CO could not be quantified) could be calibrated against those obtained on surfaces annealed at higher temperature. TPD experiments showed that the total relative yield of the volatile organic products, including CH_3COOH and CH_2CO, increased from 0.44 to 0.83 as the prior annealing tem-

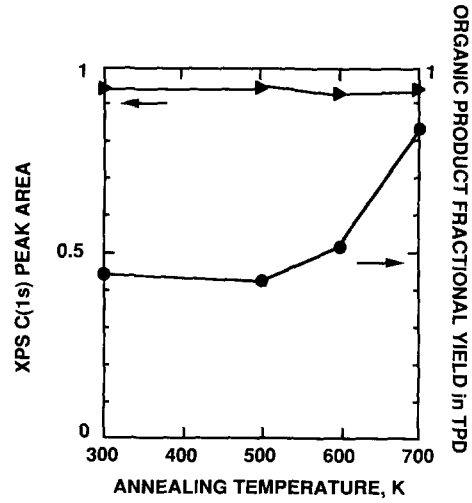

FIG. 7. C(1*s*) XPS peak area (relative to the maximum value obtained on the 750 K annealed surface) at 300 K and total fractional yield of volatile organic products from CH_3COOH decomposition on the reduced TiO_2(001) surfaces. The volatile organic products include CH_3COOH and CH_2CO.

perature was increased from 300 to 700 K. The maximum yield of volatile organic products (excluding CO) was observed to be 0.94 following CH_3COOH adsorption at 300 K on a surface which had been previously annealed to 750 K (vide infra). Since the level of surface oxidation was increased by annealing the Ar^+-bombarded surface at temperatures increasing from 300 to 700 K, these results indicate that a smaller portion of the surface acetates decomposed to deposit atomic carbon and oxygen on surfaces which were initially more highly oxidized. On the most reduced (300 K) surface, more than one CO molecule or surface carbon atom was produced on average per acetic acid molecule originally adsorbed, based upon the above calibration of the carbon balance. The signal for CO produced by carbon burn-off reactions above 650 K for the reduced surfaces became progressively flatter as the prior annealing temperature was increased, tracking the decrease in adsorbate consumption via this unselective reaction channel. The sharp increase in the relative yield of volatile organic products from the 700 K-annealed surface is clearly associated with the dramatic oxidation of the surface caused by annealing at 700 K.

2.2.2 Oxidized surfaces. As shown in Figs. 1 and 2, annealing the sputtered $TiO_2(001)$ surface at 750 K for 20 min produced the oxidized, {011}-faceted surface containing Ti^{4+} ions exclusively. Reported below are the TPD and XPS data for CH_3COOH decomposition on this {011}-faceted $TiO_2(001)$ suface.

A typical set of TPD spectra following adsorption of CH_3COOH at 300 K is displayed in Fig. 8. As in the case of the Ar^+-bombarded surface, two desorption states were observed. The peak temperatures for the desorption states were consistent with those observed on the Ar^+-bombarded surface. The lower temperature state consisted of coincident CH_3COOH and H_2O peaks at 390 K. The higher temperature state included a CH_3COOH peak at 593 K, a CO peak at 602 K, a CH_2CO peak at 610 K, and

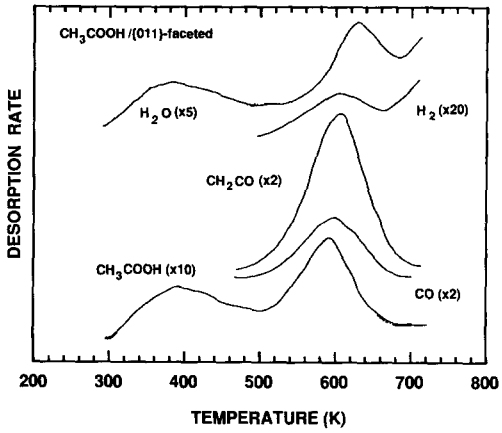

FIG. 8. TPD spectra following CH_3COOH adsorption at 300 K on the oxidized, {011}-faceted $TiO_2(001)$ surface. The spectra are uncorrected for mass spectrometer sensitivities and are offset for distinction.

an additional H_2O peak at 635 K. A very small H_2 peak which was more clearly resolved than its counterpart on the sputtered surface was observed at 610 K. The magnitudes of the CH_3COOH desorption peaks at 390 and 593 K were comparable. CH_2CO was the dominant decomposition product, appearing in an amount four times that of the CH_3COOH desorbed at 593 K. The CO desorption signal did not exhibit the rapid increase above 650 K observed on the Ar^+-bombarded surface, making possible quantification of the yields of all carbon-containing products from CH_3COOH decomposition. However, the H_2O desorption signal still increased rapidly above 650 K, precluding estimation of the yield of H_2O at 635 K. The product distribution for CH_3COOH TPD on the oxidized, {011}-faceted $TiO_2(001)$ surface is expressed in terms of molar yields in Table 2, determined on the basis of the carbon appearing in volatile products derived from surface acetates. From Table 2 a total fractional yield of 0.94 was calculated for the volatile organic products, i.e., excluding CO. This value is greater than that estimated on the 700 K-annealed surface, 0.83. The increase is attributed to the effect of surface oxidation resulting from an in-

TABLE 2

Product Distribution for CH_3COOH TPD on the {011}-faceted TiO_2(001) Surface

Product	Peak temp (K)	Molar yield per mole CH_3COOH adsorbed
CH_3COOH	390	0.15
H_2O	390	0.06
CH_3COOH	593	0.16
CO	602	0.11
CH_2CO	610	0.64
H_2	610	Trace
H_2O	635	Not quantified

crease in the prior annealing temperature by 50 K.

TPD experiments were also performed following adsorption of CH_3COOH on the {011}-faceted surface at 200 K. The results of these experiments, displayed in Fig. 9, showed that additional desorption peaks appeared below 300 K. These peaks included a CH_3COOH peak at 270 K and a H_2O peak at 285 K. The desorption state which was observed at 390 K following CH_3COOH adsorption at 300 K appeared as a shoulder around 400 K in the CH_3COOH and H_2O

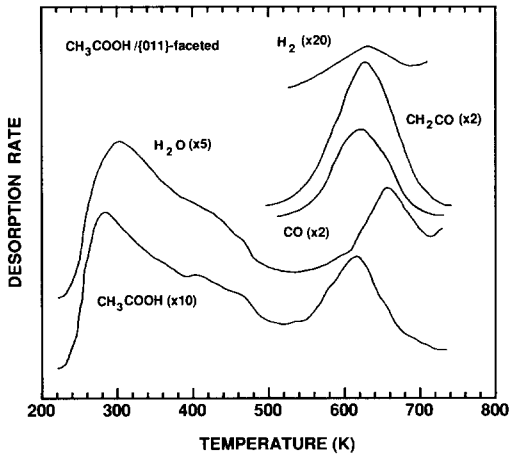

FIG. 9. TPD spectra following CH_3COOH adsorption at 200 K on the oxidized, {011}-faceted TiO_2(001) surface. The spectra are uncorrected for mass spectrometer sensitivities and are offset for distinction.

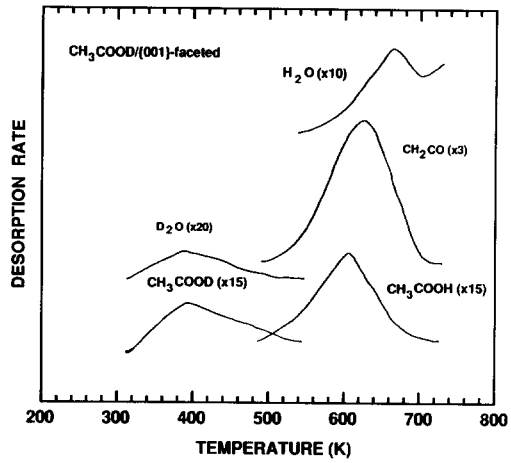

FIG. 10. TPD spectra following CH_3COOD adsorption at 300 K on the oxidized, {011}-faceted TiO_2(001) surface. The spectra are uncorrected for mass spectrometer sensitivities and are offset for distinction.

desorption spectra. The higher temperature (ca. 600 K) desorption state was relatively unaffected by reduction of the CH_3COOH adsorption temperature below 300 K. Both the desorption peak temperatures and the relative yields of the decomposition products were essentially identical, regardless of the adsorption temperature.

In order to identify the surface intermediates formed during CH_3COOH decomposition, TPD experiments following CH_3COOD adsorption at 300 K were carried out. As shown in Fig. 10, TPD spectra included CH_3COOD and D_2O peaks coincident at 390 K. The organic products desorbing at higher temperatures were CH_3COOH at 590 K and CH_2CO at 610 K. H_2O exhibited a desorption peak at 650 K. No CH_3COOD or D_2O desorption was observed above 500 K. Deuterium atoms were not incorporated into the decomposition products, as evidenced by the absence of CHDCO or CD_2CO. These results provide clear evidence that (1) the stable surface intermediates which give rise to all of the reaction products observed on the oxidized TiO_2 surface are acetate species, not acetic acid, and (2) the hydroxyls produced by dissociation of acetic acid are removed from

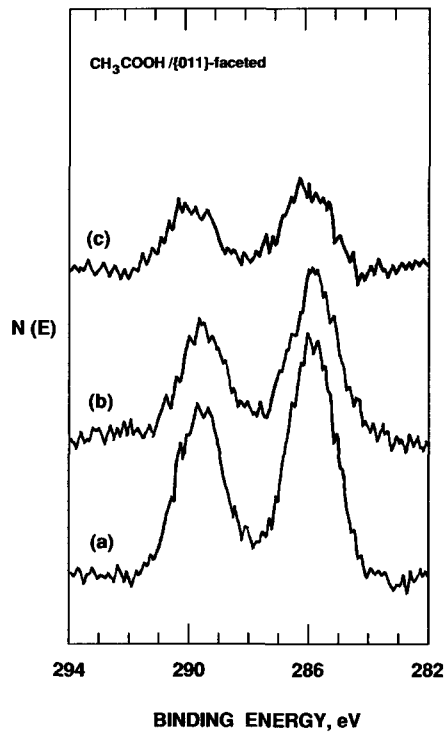

FIG. 11. C(1*s*) XPS spectra for CH_3COOH adsorbed on the oxidized, {011}-faceted TiO_2(001) surface as a function of surface temperature. (a) CH_3COOH-dosed surface at 165 K. (b) Surface in a heated to 300 K. (c) a − b difference spectrum.

the surface below 500 K. These results are in excellent agreement with those of our previous study of carboxylic acids on TiO_2 powders (*20*), which demonstrated by infrared spectroscopy and TPD that all desorption peaks at 390 K and above arose from the reactions of surface carboxylates.

These surface intermediates were probed further by XPS experiments. A typical set of C(1*s*) spectra for the CH_3COOH-dosed surface as a function of surface temperature is displayed in Fig. 11. Following CH_3COOH adsorption at 165 K, two C(1*s*) peaks centered at 289.7 and 285.9 eV were observed, as shown by curve (a) in Fig. 11. The FWHM of each C(1*s*) peak was approximately 1.8 eV. Heating the CH_3COOH-dosed surface to 300 K caused both C(1*s*) peaks to decrease in intensity and shift by 0.1 eV to lower binding energies (curve (b)). The difference between these two spectra is shown in curve (c). The C(1*s*) peaks of the difference spectrum were positioned at 290.0 and 286.0 eV, respectively. Their separation, 4.0 eV, was consistent with the separation observed in spectra of CH_3COOH in the gas phase (*33*). Owing to the low dosing temperature and the characteristic C(1*s*) peak separation, the difference spectrum can be unambiguously assigned to molecularly adsorbed acetic acid. The C(1*s*) spectrum shown in curve (b) exhibited lower binding and a smaller peak separation, 3.8 eV, as compared to molecularly adsorbed acetic acid. Due to the increased electron density around the carboxyl carbon in acetate species relative to acetic acid, a small downward shift in the C(1*s*) binding energy, along with a decrease in the C(1*s*) peak separation, occurs for adsorbed acetate species on metal oxides (*16, 34*). The peak separation in curve (b) was comparable to those reported for adsorbed acetate species on ZnO (*16*), 3.6 eV, and for sodium acetate (*33*), 3.7 eV. These XPS results, together with CH_3COOD TPD results, demonstrate that the stable surface intermediates at 300 K on the oxidized TiO_2 single crystal are adsorbed acetates. Thus, it can be deduced that exposure of the oxidized TiO_2 surface to CH_3COOH at 165 K resulted in both molecular and dissociative adsorption. Upon heating, the molecularly adsorbed species desorbed readily, as evidenced by the CH_3COOH desorption peak at 270 K in Fig. 8.

These conclusions are further supported by the O(1*s*) spectra. As shown in Fig. 12a, a typical O(1*s*) spectrum following CH_3COOH adsorption at 165 K exhibited two notable features compared to that of the clean surface. First, the O(1*s*) peak at 530.7 eV was attenuated due to the presence of adsorbates. (The O(1*s*) spectrum of the clean surface is indicated by the dotted line in Fig. 12a.) A similar attenuation was also observed in the Ti(2*p*) spectrum. These attenuations accompanying the coverage of

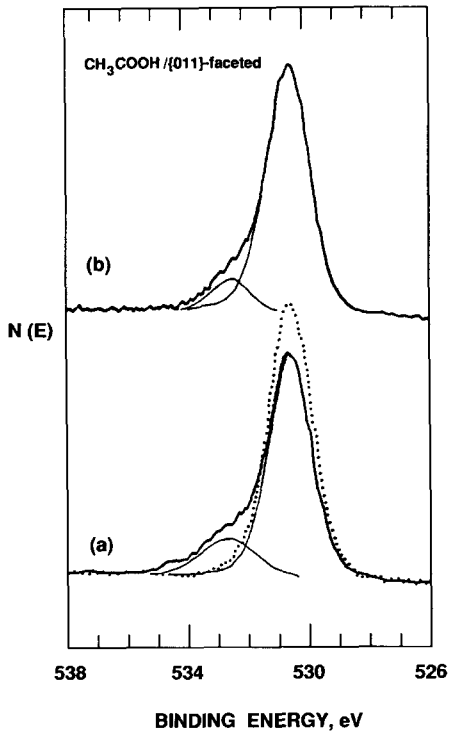

FIG. 12. O(1*s*) XPS spectra for CH_3COOH adsorbed on the oxidized, {011}-faceted TiO_2(001) surface as a function of surface temperature. (a) CH_3COOH-dosed surface at 165 K. The dotted line indicates the O(1*s*) spectrum for the clean surface. (b) Surface in a heated to 300 K.

the TiO_2 surface with adsorbates could be reversed by heating the surface above 700 K, by which temperature most of the adsorbates were removed from the surface. Second, an additional O(1*s*) peak appeared at higher binding energy as evidenced by the shoulder positioned around 533 eV. By curve-fitting, the O(1*s*) spectrum could be decomposed into the lattice oxygen peak at 530.7 eVand a broad adsorbate oxygen peak at 532.6 eV. The separation between these two peaks, 1.9 eV, was consistent with that reported for molecularly adsorbed HCOOH on a TiO_2(110) single crystal (*35*).The FWHM of the adsorbate oxygen peak was 2.2 eV. Heating the CH_3COOH-dosed surface to 300 K resulted in a reduction in the intensity of the adsorbate oxygen peak as well as the partial recovery of the intensity of the lattice oxygen peak (Fig. 12b.). Curve-fitting showed that the adsorbate oxygen peak shifted by 0.2 eV to lower binding energy and the FWHM of the peak decreased by 0.7 eV. Heating the surface to 425 K reduced the adsorbate oxygen peak further; however, no binding energy shift was observed. Comparison of the adsorbate oxygen peaks at 165 and 300 K with respect to FWHM and binding energy showed that the adsorbate oxygen peak at 300 K represented a single type of oxygen atom whereas the adsorbate oxygen peak at 165 K must represent two different oxygen atoms. This is consistent with the usual XPS observation that adsorbed acetates have two equivalent oxygen atoms whereas molecularly adsorbed acetic acid has two nonequivalent oxygen atoms (*36*, *37*). These results also demonstrate that the surface intermediates at 300 K were adsorbed acetates, while molecularly adsorbed acetic acid was also present at 165 K. Acetic anhydride was excluded from the possible surface species on the basis of the relatively low binding energy and the narrow width of the adsorbate oxygen peaks (*34*).

Following adsorption of CH_3COOH at 300 K, two C(1*s*) peaks centered at 289.6 and 285.8 eV were observed as displayed by curve (a) in Fig. 13. These binding energies were consistent with those observed following adsorption at 165 K plus heating to 300 K, shown by curve (b) in Fig. 11. The FWHM of each C(1*s*) peak was 1.8 eV. The ratio of the area of the carboxylate carbon peak to the area of the methyl group carbon peak was 0.85. These values are consistent with those obtained with this instrument for adsorbed acetate species on zinc oxide (*16*). The total area of the C(1*s*) peaks was comparable to that observed in the case of the Ar^+-bombarded surface, indicative of the equal coverage of the surface intermediates formed by CH_3COOH adsorption at 300 K on the two surfaces. Heating the CH_3COOH-dosed surface to 425 K reduced the C(1*s*) peak area by roughly 20% (curve(b),

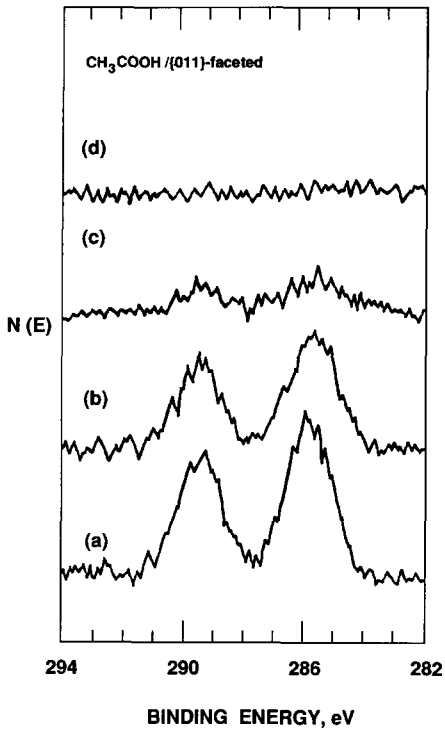

FIG. 13. C(1*s*) XPS spectra for CH_3COOH adsorbed on the oxidized, {011}-faceted TiO_2(001) surface as a function of surface temperature. (a) CH_3COOH-dosed surface at 300 K. (b) Surface in a heated to 425 K. (c) Surface in b heated to 600 K. (d) Surface in c heated to 650 K.

Fig. 13), consistent with the determination from TPD results that 15% of the adsorbed acetates were removed as CH_3COOH at 390 K. The FWHM of the carboxylate carbon peak decreased by 0.3 eV upon heating to 425 K while that of the methyl group did not change. No binding energy shift was observed. The difference between the C(1*s*) spectra at 300 and 425 K exhibited no evidence for molecularly adsorbed acetic acid, but only for adsorbed acetate species. Heating the surface to 500 and 550 K resulted in the progressive diminution of the C(1*s*) peaks; however, no binding energy shifts were observed. Heating the surface to 600 K caused the C(1*s*) peaks to shift by 0.1 eV to lower binding energy and to decrease significantly in area (curve(c), Fig. 13). The decrease in the C(1*s*) peak area was consistent with the TPD results, which showed that the evolution of acetate decomposition products began near 470 K and peaked around 600 K. However, the C(1*s*) spectrum in curve (c) showed that a substantial portion of the adsorbed acetate species remained on the surface after heating to 600 K. These remaining acetates were completely removed from the surface by heating to 650 K (curve (d), Fig. 13), thereby producing a clean surface. These results are strikingly different from those in the case of the Ar^+-bombarded surface described above. These XPS results, together with the TPD results showing an increase in the total yield of volatile organic products on the more heavily oxidized TiO_2 surface, clearly demonstrate that the adsorbed acetate species are more thermally stable on the oxidized surface than on the oxygen-deficient surface.

It was demonstrated in Figs. 1 and 2 that the oxygen concentration in the region sampled by AES and XPS increased further as the prior annealing temperature was increased above 750 K. Accompanying this increase was a transition in surface structure from {011} facets to {114} facets. TPD and XPS experiments with acetic acid on these highly oxidized, faceted surfaces exhibited several notable features. First, for the 850 K-annealed surface a desorption peak for an additional product, acetone, was observed at 580 K. The fractional yield of CH_3COCH_3 increased progressively as the prior annealing temperature was increased. On the other hand, the fractional yield of the dominant decomposition product, CH_2CO, decreased progressively as the prior annealing temperature was increased. These results demonstrate that the selectivity of CH_3COOH decomposition on TiO_2 is dependent on the structure and composition of the surface. Second, the effect of annealing on surface activity was less dramatic than on selectivity. The total yield of volatile organic products remained nearly constant in going from the 750 K-annealed, {011}-faceted surface to

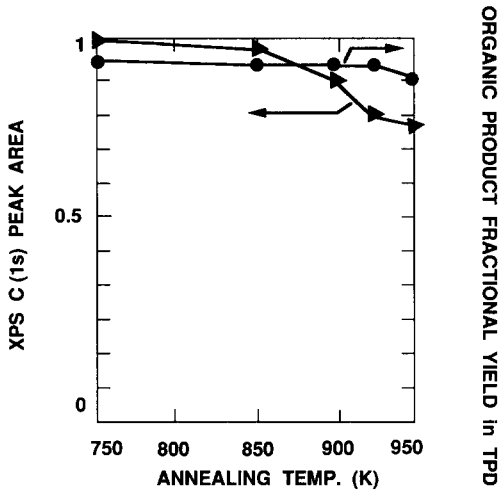

FIG. 14. C(1*s*) XPS peak area at 300 K and fraction of acetates desorbed as volatile organic products from CH_3COOH decomposition on the oxidized TiO_2(001) surfaces. The volatile organic products include CH_3COOH, CH_2CO, and CH_3COCH_3.

the 950 K, {114}-faceted surface. Meanwhile, the C(1*s*) peak area following CH_3COOH adsorption at 300 K was comparable for the 750- and 850 K-annealed surfaces, but decreased by 20% for surfaces annealed above 900 K. In Fig. 14 are displayed the relative coverages of surface intermediates formed by CH_3COOH adsorption at 300 K and the fraction of the total carbon converted to volatile organic products for each oxidized surface. Below are reported TPD and XPS data obtained from CH_3COOH decomposition on the more completely oxidized, {114}-faceted TiO_2(001) surface formed by annealing at 950 K.

Figure 15 displays a typical set of TPD spectra obtained following CH_3COOH adsorption at 300 K on the {114}-faceted TiO_2(001) surface. As in the cases of the Ar^+-bombarded surface and the 750 K-annealed, {011}-faceted surface, two desorption states were observed. The lower temperature state consisted of CH_3COOH and H_2O peaks at 395 K. The higher temperature state included the desorption peaks for CH_3COOH at 605 K, CO at 610 K, CH_2CO at 630 K, and additional H_2O at 660 K. Most striking, however, was the CH_3COCH_3 peak at 580 K. This additional organic product, which was a major product from CH_3COOH TPD on polycrystalline anatase powders (*20*), was not observed on either the Ar^+-bombarded surface or the 750 K-annealed, {011}-faceted surface. A very small H_2 peak was also observed at 630 K. A small additional CO peak, which was not observed on the {011}-faceted surface, was observed at 780 K. The yields of CH_3COOH at 395 and 605 K were comparable. CH_2CO was still the dominant decomposition product. The product distribution for CH_3COOH TPD on the oxidized, {114}-faceted TiO_2(001) surface is listed in Table 3.

XPS experiments were conducted on the {114}-faceted TiO_2 surface following adsorption of CH_3COOH at 300 K. As displayed by curve (a) in Fig. 16, C(1*s*) peaks were centered at 289.6 and 285.8 eV as was typical of adsorbed acetate species on oxidized TiO_2 surfaces. The C(1*s*) peak area was approximately 77% of that obtained following adsorption on the 750 K-annealed, {011}-faceted surface, indicative of a decrease in the saturation adsorbate coverage. Heating the CH_3COOH-dosed surface to 425 K reduced the intensity of the C(1*s*) peaks by approxi-

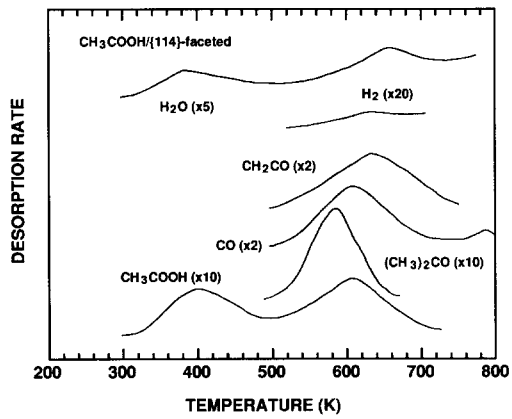

FIG. 15. TPD spectra following CH_3COOH adsorption at 300 K on the oxidized, {114}-faceted TiO_2(001) surface. The spectra are uncorrected for mass spectrometer sensitivities and are offset for distinction.

TABLE 3

Product Distribution for CH_3COOH TPD on the {114}-faceted TiO_2(001) Surface

Product	Peak temp (K)	Molar yield per mole CH_3COOH adsorbed
CH_3COOH	395	0.13
H_2O	395	0.03
CH_3COCH_3	580	0.09
CH_3COOH	605	0.16
CO	610	0.18
CH_2CO	630	0.47
H_2	630	trace
H_2O	660	0.03
CO	780	0.02

mately 20% (curve (b)), which is reasonably consistent with the fractional yield of CH_3COOH at 395 K. The carboxyl peak shifted by 0.1 eV to higher binding energy, while no binding energy shift was observed for the methyl peak. Heating the surface to 550 K resulted in attenuation of the C(1*s*) peaks as well as notable changes in the C(1*s*) binding energies (curve (c)). A further upward shift by 0.2 eV was observed for the carboxyl peak; this peak was centered at 289.9 eV. The methyl peak appeared to shift downward by 0.2 eV to 285.6 eV. Thus the peak separation increased to 4.3 eV, 0.5 eV greater than the value for adsorbed acetate species. This result indicates that the surface intermediates at 550 K on the {114}-faceted surface consisted of other carbon-containing species in addition to the acetates. The apparent shift of the carboxyl carbon peak to higher binding energy may reflect a contribution from surface carbonate species, while the apparent shift of the methyl group carbon peak to lower binding energy is due to formation of adsorbed atomic carbon. Since the carbon atom in carbonate species has one more oxygen atom attached than does a carboxylate carbon, a carbon atom in a surface carbonate would be more electron-deficient and would be expected to exhibit a higher C(1*s*) binding energy relative to the carboxylate carbon. Barteau and Madix (*38*) have reported that the binding energy of the C(1*s*) peak of carbonate species on Ag(110) was 0.5 eV greater than that of carboxylates. Assuming the same binding energy shift in this study, the surface carbonate species on TiO_2 would have a C(1*s*) binding energy of 290.1 eV, which is close to the higher binding energy peak in the C(1*s*) spectrum at 550 K. A value of 290.1 eV is slightly higher than the values reported by Tanaka *et al.* (*32*) for stable carbonates on TiO_2 powders, but is in good agreement with the value for nickel carbonate (*39*). One important observation derived from XPS and TPD data is that surface carbonate species in the spectrum at 550 K are most likely associated with the desorption of CH_3COCH_3 at 580 K. The proposed formation of surface carbonate species via bimolecular ketonization of adsorbed acetate species has been discussed previously for

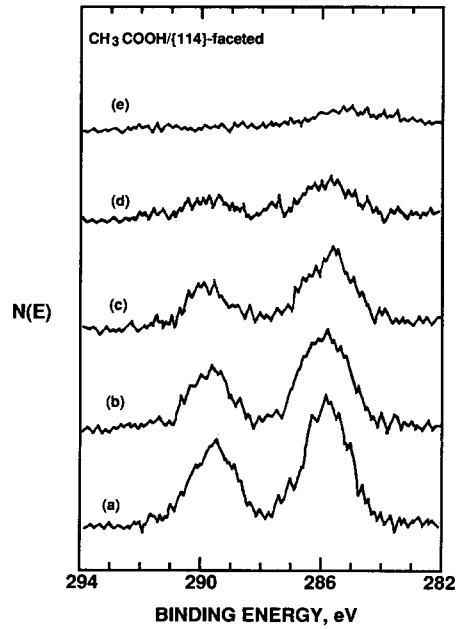

FIG. 16. C(1*s*) XPS spectra for CH_3COOH adsorbed on the oxidized, {114}-faceted TiO_2(001) surface as a function of surface temperature. (a) CH_3COOH-dosed surface at 300 K. (b) Surface in a heated to 425 K. (c) Surface in b heated to 550 K. (d) Surface in c heated to 650 K. (e) Surface in d heated to 750 K.

results obtained on polycrystalline anatase powders (*20*).

Acetate intermediates could be removed by heating the surface to 650 K; however, a substantial portion of the surface intermediates remained as evidenced by the C(1*s*) peak intensities of curve (d) in Fig. 16. This is notably different from the case of the 750 K-annealed, {011}-faceted surface which was devoid of any adsorbates at 650 K. Indeed TPD spectra for the {114}-faceted surface exhibited ca. 10 to 20 K increases in peak temperature for acetate decomposition products compared to those on the {011}-faceted surface. These XPS and TPD results indicate that adsorbed acetates possess greater thermal stability on the more highly oxidized, {114}-faceted surface. Heating the surface to 750 K resulted in complete removal of the adsorbed acetate species as well as of the surface carbonate species, as evidenced by the flat C(1*s*) XPS signal above 287 eV. However, the presence of a small C(1*s*) peak at 284.0 eV demonstrated that residual carbon remained on the surface. This is consistent with the TPD results showing no desorption peaks of organic products above 750 K but a small CO peak at 780 K. This CO desorption was undoubtedly due to burn-off of the adsorbed atomic carbon via reaction with the lattice oxygen of the TiO_2 surface.

2.2.3 Selectivity of CH_3COOH decomposition on TiO_2 (001) surfaces. The TPD and XPS data described above demonstrate that the selectivity of CH_3COOH decomposition on TiO_2(001) is dependent on both surface composition and structure. This dependence is displayed in summary form in Fig. 17. The product selectivities plotted in this figure were calculated on the basis of the fraction of the carbon originally present in surface acetates appearing in each of the products; i.e., it reflects the tabulated molar yields corrected for product stoichiometry. On the highly reduced, Ar^+-bombarded surface, the adsorbed acetate species reacted mainly via unselective decomposition to

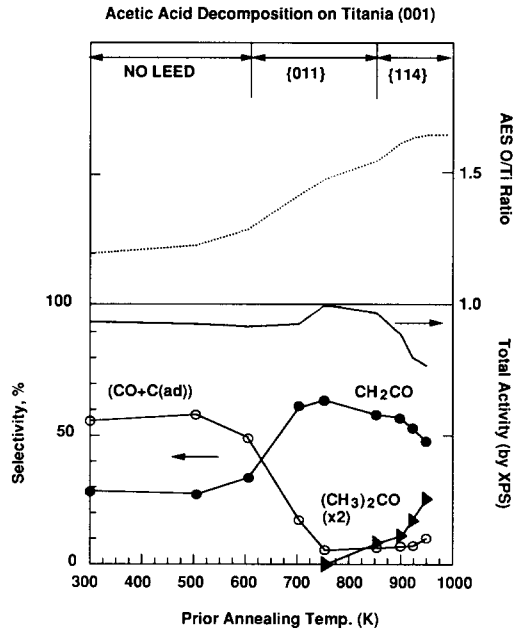

FIG. 17. Selectivity of CH_3COOH decomposition on TiO_2(001) surfaces. The selectivity is defined as the fraction of the total carbon appearing in each product.

produce surface oxidation, as evidenced by the high selectivity (56%) for CO plus adsorbed atomic carbon. As the surface was progressively oxidized by prior annealing, the selectivity for CH_2CO increased while the selectivity for CO plus adsorbed carbon decreased. The selectivity for CH_2CO reached a maximum value of 64% on the 750 K-annealed, {011}-faceted surface. As the surface was further oxidized and faceted by increasing the prior annealing temperature above 750 K, the selectivity for CH_2CO gradually decreased while an additional product, CH_3COCH_3, was produced with increasing selectivity. The selectivities for CH_2CO and CH_3COCH_3 were 47 and 13%, respectively, for the 950 K-annealed, {114}-faceted surface. The selectivity for CO plus adsorbed atomic carbon, which reached a minimum value of 5% for the 750 K-annealed, {011}-faceted surface, gradually increased to 10% for the 950 K-annealed,

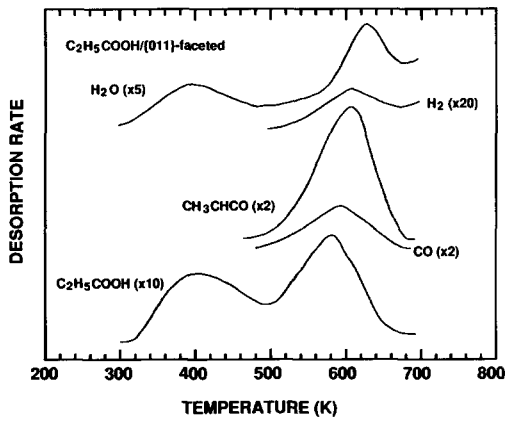

FIG. 18. TPD spectra following C_2H_5COOH adsorption at 300 K on the oxidized, {011}-faceted $TiO_2(001)$ surface. The spectra are uncorrected for mass spectrometer sensitivities and are offset for distinction.

{114}-faceted surface. The total activity of the surface for dissociative adsorption of CH_3COOH remained relatively constant for surfaces annealed at 850 K and below, but decreased by ca. 20% for the surface annealed above this temperature.

2.3 C_2H_5COOH Decomposition

In order to investigate whether the chemistry of CH_3COOH decomposition could be extended to higher carboxylic acids, C_2H_5COOH decomposition was performed on the 750 K-annealed, {011}-faceted surface as well as on the 950 K-annealed, {114}-faceted surface. The results of C_2H_5COOH TPD experiments on these faceted TiO_2 surfaces were indeed analogous to those obtained for CH_3COOH TPD.

Figure 18 displays a typical set of TPD spectra obtained following adsorption of C_2H_5COOH at 300 K on the 750 K-annealed, {011}-faceted surface. As in the case of CH_3COOH TPD, two principal desorption states were observed. The lower temperature state consisted of coincident C_2H_5COOH and H_2O peaks at 390 K. These peak temperatures were consistent with those observed from experiments on polycrystalline anatase powders (*20*). The higher temperature state included an additional C_2H_5COOH peak at 580 K, a CO peak at 595 K, a CH_3CHCO (methyl ketene) peak at 608 K, and an additional H_2O peak at 628 K. A very small H_2 peak was also observed at 608 K. As in the case of CH_3COOH TPD, the H_2O desorption signal increased rapidly above 650 K; thus the yield of H_2O could not be determined reliably. The desorption of C_2H_4, if any, could not be resolved, as this molecule has primary cracking fragments of *m/e* 28, 27, and 26 which overlap fragments from other products, including methyl ketene. The dominant decomposition product at 608 K, methyl ketene, was identified on the basis of the peak area analysis and the cracking pattern of an isomer, acrolein. As presented in Table 4, the peak areas for the higher temperature desorption state which remained after subtraction of the contributions from C_2H_5COOH and CO were not consistent with the acrolein cracking pattern obtained with the same mass spectrometer. Especially important is the lack of consistency for *m/e* 29, which is a major characteristic fragment of aldehydes, representing the -CHO group. Thus, although the mass spectral data for methyl ketene were not available in the literature, the high-temperature decomposition product was assigned to methyl ketene, the C_3-homolog of ketene formed from CH_3COOH TPD. The peak temperature of methyl ketene, 608 K as determined from the *m/e* 55 and 56 spectra, was nearly identical to that of ketene observed from CH_3COOH TPD. The C_2H_5COOH TPD data obtained on polycrystalline powders (*20*) were more ambiguous in the resolution of methyl ketene and acrolein. If methyl ketene were the product formed, it would not be expected to isomerize to acrolein before being detected by the mass spectrometer in studies with a single crystal in ultrahigh vacuum. On polycrystalline powders, the product methyl ketene may be isomerized to the thermodynamically preferred acrolein via an intramolecular hydrogen shift (*40, 41*) upon reencountering TiO_2 surfaces, given the higher operating pressures of those experiments

TABLE 4

Peak Area Analysis of C_2H_5COOH TPD Data for the Higher Temperature Desorption State from the {011}-faceted Surface; Peak Area is Expressed in Arbitrary Units

m/e	Peak temp (K)	Peak area	C_2H_5COOH desorption	CO desorption	Remainder	Acrolein cracking
26	607	80	6		74	46
27	606	94	12		82	78
28	600	148	17	31	100	100
29	584	15	12		3	44
45	580	5	5		0	0
55	608	15	1		14	24
56	608	62	2		60	30
74	580	4	4		0	0

and the high surface area of the powder samples. Other molecules which were checked for but not detected included $(C_2H_5)_2CO$, CO_2, CH_2CO, C_2H_6, and C_3–C_4 alkenes and alkanes. The product distribution for C_2H_5COOH TPD on the {011}-faceted TiO_2(001) single crystal is listed in Table 5.

Two C(1*s*) peaks centered at 289.5 and 285.7 eV were observed following adsorption of C_2H_5COOH; as in the spectra of acetates, the high binding energy peak can be assigned to the carboxyl carbon, while the low binding energy peak can be assigned to the alkyl carbons. The binding energies as well as the peak separation, 3.8 eV, were typical of adsorbed carboxylate species on TiO_2. The ratio of the area of the carboxylate peak to that of the alkyl peak was 0.38, smaller than the value of 0.5 which would be expected for propionate species. The deviation of this ratio from the stoichiometric value is most likely due to the screening of the carboxylate carbon by the alkyl carbons. The ratio is consistent with the value obtained with this instrument for propionates on ZnO (*16*). Heating the C_2H_5COOH-dosed surface to 425 K attenuated the C(1*s*) peaks by ca. 20% (curve (b), Fig. 19), consistent with the fractional yield of 0.14 for the C_2H_5COOH desorption peak at 390 K. Heating the surface to 500 and 550 K progressively attenuated the C(1*s*) peaks by causing the loss of adsorbed propionate species; however, no binding energy shifts were observed during these heat treatments. Heating the surface to 600 K resulted in a significant decrease in the C(1*s*) peak area, consistent with the TPD peaks for the propionate decomposition products around 600 K. The C(1*s*) peaks shifted to lower binding energies, i.e., 289.4 and 285.4 eV, respectively. Similar binding energy shifts were also observed in the course of CH_3COOH conversion. Upon heating the surface to 650 K, the adsorbed propionate species were completely removed as demonstrated by the flat C(1*s*) spectrum typical of a clean surface. These XPS results were analogous to those obtained for CH_3COOH.

For the 950 K-annealed, {114}-faceted

TABLE 5

Product Distribution for C_2H_5COOH TPD on the {011}-faceted TiO_2(001) Surface

Product	Peak temp (K)	Molar yield per mole C_2H_5COOH adsorbed
C_2H_5COOH	390	0.14
H_2O	390	0.04
C_2H_5COOH	580	0.16
CO	595	0.09
CH_3CHCO	608	0.67
H_2	608	Trace
H_2O	628	Not quantified

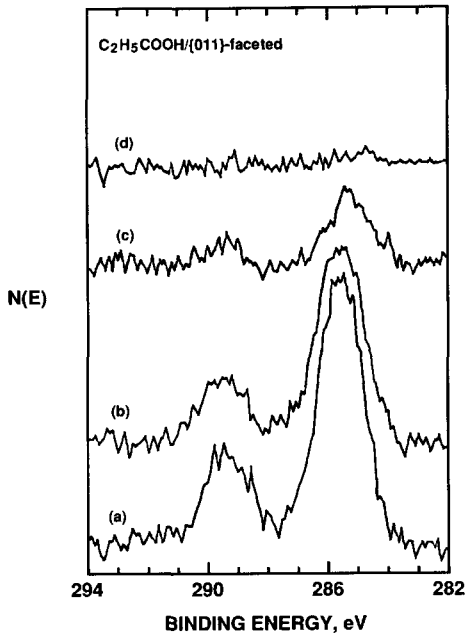

FIG. 19. C(1*s*) XPS spectra for C_2H_5COOH adsorbed on the oxidized, {011}-faceted TiO_2(001) surface as a function of surface temperature. (a) C_2H_5COOH-dosed surface at 300 K. (b) Surface in a heated to 425 K. (c) Surface in b heated to 600 K. (d) Surface in c heated to 650 K.

surface, TPD experiments performed following adsorption of C_2H_5COOH at 300 K gave rise to results consistent with those obtained from CH_3COOH TPD on the same surface; the homologous dialkyl ketone was observed among the propionate decomposition products. The formation of this additional decomposition product, 3-pentanone, at 590 K was evidenced by increased peak intensities for *m/e* 57 and 29 at 590 K. *m/e* 29 is the primary cracking fragment for 3-pentanone, and *m/e* 57 corresponding to $C_2H_5CO^+$ is the fragment characteristic of 3-pentanone obtained from fragmentation at the acyl carbon of the dialkyl ketone. (For acetone formed from CH_3COOH TPD, *m/e* 43 corresponding to CH_3CO^+ is the primary fragment.) The yield of 3-pentanone corresponded to roughly 5% of the total propionate coverage on the {114}-faceted surface at 300 K. A decrease in the fractional yield of CH_3CHCO (the unimolecular reaction product) from 0.65 to 0.59 was observed to coincide with the appearance of 3-pentanone (the bimolecular reaction product). These TPD and XPS data demonstrate that the decomposition of CH_3COOH and C_2H_5COOH on TiO_2 can be explained by common reaction pathways.

DISCUSSION

The results of this study clearly demonstrate that the selectivity of the conversion of higher carboxylic acids on TiO_2 is sensitive to the structure and composition of the surface. Three principal reaction channels were observed as the surface was annealed to produce progressive oxidation and faceting: unselective deoxygenation on the reduced surface, selective unimolecular dehydration on the {011}-faceted (001) surface, and bimolecular ketonization on the {114}-faceted (001) surface. All of these reactions proceeded via the initial dissociative adsorption to form adsorbed carboxylate species. Ironically, the activity of the TiO_2(001) surface for carboxylate formation was not strongly influenced by the changes in composition and structure which had such a dramatic effect on selectivity. Dissociation of carboxylic acids on metal oxides appears to require only accessible cation–anion site pairs on the surface, with the conjugate base of the parent acid bound at a coordination vacancy of the metal cation. This description is in accord with the interpretation of previous studies of adsorption on TiO_2 powders (*42, 43*) and with observations from this laboratory of the site requirements for carboxylic acid dissociation on single crystal surfaces of other oxides (*3, 14, 16, 44*). The various TiO_2 surfaces considered in this study exhibit comparable capacities for dissociation of acetic acid; only when fully coordinated Ti cations are created by {114}-faceting does the initial acetate coverage decline.

The mechanism of acetic acid decomposition to the various products observed in this study was largely deduced in our previous report of acetic acid TPD on polycrystalline

TiO_2 powders (*20*). This sequence may be summarized as follows (O(ℓ) represents lattice oxygen at the surface):

(1) $CH_3COOH(g) + O(\ell) \rightarrow CH_3COO(ad) + OH(ad)$

(2) $CH_3COO(ad) + OH(ad) \xrightarrow{390K} CH_3COOH(g) + O(\ell)$

(3) $2OH(ad) \xrightarrow{390K} H_2O(g) + O(\ell)$

(4) $2CH_3COO(ad) \xrightarrow{580K} CH_3COCH_3 + CO_3(ad)$

(5) $CO_3(ad) \rightarrow CO, CO_2 + O(\ell)$

(6) $CH_3COO(ad) \xrightarrow{600K} CH_3(ad) + CO(g) + O(\ell)$

(7) $CH_3(ad) \rightarrow CH_4(g), C(ad), H(ad)$

(8) $CH_3COO(ad) \xrightarrow{610K} CH_2CO(g) + H(ad) + O(\ell)$

(9) $CH_3COO(ad) + H(ad) \rightarrow CH_3COOH(g)$

(10) $2H(ad) (+O(\ell)) \rightarrow H_2, H_2O$

(11) $C(ad) + O(\ell) \xrightarrow{>600K} CO(g)$

Steps 5, 7, and 10 represent the rapid consumption of unstable intermediates produced by acetate decomposition and are clearly not elementary processes. What could not be determined from the powder work was the structural dependence of these reactions and the identity of the surface sites on which a common intermediate, the acetate, reacts to form these products. The single-crystal results resolve the nature of these sites and, when compared with results from other single crystals, permit some important generalizations relevant to catalysis by metal oxides.

Dissociative adsorption and net unimolecular dehydration of carboxylic acids appear to require only a single coordination vacancy on the part of the surface cations. As shown in Fig. 17, acetates react to form ketene on the oxidized {011}-faceted surface with high selectivities (>60%). This observation is quite consistent with results from the ZnO(0001) and MgO(100) surfaces. These surfaces also expose cations with a single coordination vacancy; they yield ketene (and no acetone) as the principal product of selective acetate decomposition (*16, 44*). It should be emphasized that this net dehydration occurs not via acid catalysis, but via proton abstraction at surface base sites (oxygen anions) to form adsorbed carboxylates. Thus one can achieve quite high selectivities for dehydration via base-catalyzed reaction sequences. A principal factor in the dehydration (vs decarboxylation) selectivity of carboxylic acids on oxides appears to be the reducibility of the oxide. Even if the initial dissociative adsorption removes lattice oxygen to form water, the reaction of acetates to ketene can restore this oxygen; dehydration is not a net consumer of lattice oxygens. In our single-crystal studies the highest selectivities for carboxylic acid dehydration have been achieved on the oxide which is the most basic and least reducible, MgO (*44*).

In contrast, the bimolecular ketonization of carboxylates is a more structurally demanding and less ubiquitous reaction on oxide surfaces. This reaction appears to require a pair of coordination sites on a common cation. These are provided only by the fourfold oxygen-coordinated Ti^{4+} sites of the {114}-faceted TiO_2(001) surface in this study. This reaction does not occur on the fivefold coordinated sites of the {011}-faceted surface; likewise, it does not occur on the ZnO(0001) or MgO(100) surfaces as these also do not exhibit doubly coordinatively unsaturated cations (*16, 44*). As we have previously suggested from our studies of TiO_2 powders (*20*), ketonization occurs via the coupling of a pair of carboxylate intermediates; it does not require the participation of molecular acetic acid as has been suggested in other work (*45*). This conclusion is suggested by IR spectra from powders, by XPS spectra from single crystals, and by the absence of adsorbed or gaseous CH_3COOH in these ultrahigh vacuum TPD experiments. It is also consistent with the structure-sensitivity of the ketonization reaction: coupling of a pair of carboxylates

requires a pair of sites which individually are capable of binding one of these species. The oxidation state of the surface also plays a role in this reaction. Although highly coordinatively unsaturated Ti cations were undoubtedly present on the sputtered, unannealed TiO_2(001) surface, this surface exhibited no evidence for ketone formation. Owing to its reduced state, this surface showed a strong tendency to deoxygenate adsorbates (and thereby become oxidized); this channel dominated all others on this surface. *Thus the ketonization of carboxylic acids appears to require doubly coordinatively unsaturated cations on a fully oxidized surface.*

This site requirement for ketonization of carboxylates is directly analogous to that for Ziegler–Natta polymerization of olefins (*46*). Classical Ziegler–Natta catalysts are prepared from α-$TiCl_3$ and metal alkyls like $Al(C_2H_5)_3$. In solid $TiCl_3$, the Ti^{3+} cations are octahedrally coordinated, as are the Ti^{4+} cations in the TiO_2 rutile structures. The titanium cations on which olefin polymerization takes place are coordinatively unsaturated. Polyolefin formation is considered to be initiated by a ligand exchange of $TiCl_3$ with $Al(C_2H_5)_3$: $Al(C_2H_5)_3 + TiCl_3 \rightarrow Al(C_2H_5)_2Cl + TiCl_2(C_2H_5)$. Adding an olefin ligand to the coordinatively unsaturated Ti^{3+} cations on the $TiCl_2(C_2H_5)$ leads to the formation of a σ-bonded alkyl incorporating the new monomer unit (olefin ligand). Evidence for such reactions on TiO_2 has been reported in the literature. The formation of butene via coupling of ethylene is a relevant example of the oligomerization on titania (*24, 47*). The reaction of acetylene to form benzene via polyacetylene (*48–50*) as well as the reaction of methyl acetylene to form hydrocarbons of larger carbon number (*51*) also demonstrates the oligomerization capability of TiO_2 surfaces. The oligomerization or polymerization activity of TiO_2 can be best interpreted in terms of the coordination chemistry of surface Ti cations, as is the reaction mechanism for Ziegler–Natta polymerization (*46, 52*). If anything, the coupling of a pair of carboxylates to form a ketone plus a surface carbonate is a more complex reaction than the coupling of a pair of olefins. The latter requires only a migratory insertion into the cation-alkyl bond; the former must involve at minimum transfer of an alkyl ligand from one carboxylate and of an oxygen atom from the other. One can hypothesize that ketonization of carboxylic acids might therefore serve as an interesting probe of olefin polymerization catalysts. Beyond the hypothetical, this study clearly demonstrates that the active sites for oligomerization reactions can be identified from studies of well-defined surfaces under UHV conditions.

CONCLUSIONS

Acetate species were the stable intermediates formed by acetic acid adsorption on TiO_2(001) single crystal surfaces. The surface acetates were removed via two channels: recombination with surface hydroxyl species at 390 K and decomposition at higher temperatures. The decomposition selectivity was dependent on the surface structure and composition. While the sputtered, oxygen-deficient surface favored direct deoxygenation of surface acetates to produce surface oxidation accompanied by carbon deposition, the oxidized surfaces favored acetate decomposition to volatile organic products. Surface acetates decomposed exclusively via net unimolecular dehydration to CH_2CO on the {011}-faceted surface containing fivefold oxygen-coordinated Ti cations. On the {114}-faceted surface bimolecular ketonization to produce CH_3COCH_3 was also observed. The limitation of this bimolecular reaction to the {114}-faceted surface clearly demonstrates that ketonization requires the coordination of two acetates to a common titanium cation on a stoichiometric surface. Of the single-crystal surfaces examined, only the {114}-faceted surface met this requirement.

ACKNOWLEDGMENTS

We gratefully acknowledge the support of the National Science Foundation (Grant CBT-8714416) for this research.

REFERENCES

1. Boudart, M., and Djega-Mariadassou, "Kinetics of Heterogeneous Catalytic Reactions." Princeton University Press, Princeton, NJ, 1984.
2. Volta, J. C., and Portefaix, J. L., *Appl. Catal.* **18,** 1 (1985).
3. Barteau, M. A., and Vohs, J. M., *in* "Successful Design of Catalysts" (T. Inui, Ed.), p. 89. Elsevier, Amsterdam, 1988.
4. Machiels, C. J., Cheng, W. H., Chowdhry, U., Farneth, W. E., Hong, F., McCarron, E. M., and Sleight, A. W., *Appl. Catal.* **25,** 249 (1986).
5. Farneth, W. E., Staley, R.H., and Sleight, A. W., *J. Amer. Chem. Soc.* **108,** 2327 (1986).
6. Tatibouet, J. M., and Germain, J. E., *J. Catal.* **72,** 375 (1981).
7. Tatibouet, J. M., Germain, J. E., and Volta, J. C., *J. Catal.* **82,** 240 (1983).
8. Mingot, B., Floquet, N., Betrand, O., Treilleux, M., Heizmann, J. J., Massardier, J., and Abon, M., *J. Catal.* **118,** 424 (1989).
9. Volta, J. C., and Tatibouet, J. M., *J. Catal.* **93,** 467 (1985).
10. Volta, J. C., Tatibouet, J. M., Phichitkul, C., and Germain, J. E., *in* "Proceedings, 8th International Congress on Catalysis, Berlin, 1984," Vol. 4, p. 451. Dechema, Frankfurt-am-Main, 1984.
11. Brückman, K., Garbowski, R., Haber, J., Mazurkiewics, A., Sloczynski, J., and Wiltkowski, T., *J. Catal.* **104,** 71 (1987).
12. Bowker, M., Houghton, H., Waugh, K. C., Giddings, T., and Green, M., *J. Catal.* **84,** 252 (1983).
13. Djega-Mariadassou, G., Davignon, L., and Marques, A. R., *J. Chem. Soc. Faraday Trans.* 1 **78,** 2447 (1982).
14. Vohs, J. M., and Barteau, M. A., *Surf. Sci.* **176,** 91 (1986).
15. Vohs, J. M., and Barteau, M. A., *J. Phys. Chem.* **91,** 4766 (1987).
16. Vohs, J. M., and Barteau, M. A., *Surf. Sci.* **201,** 481 (1988).
17. Vohs, J. M., and Barteau, M. A., *Surf. Sci.* **221,** 590 (1989).
18. Zwicker, G., Jacobi, K., and Cunningham, J., *Int. J. Mass Spectrosc. Ion Processes* **60,** 213 (1984).
19. Akhter, S., Lui, K., and Kung, H. H., *J. Phys. Chem.* **89,** 1958 (1984).
20. Kim, K. S., and Barteau, M. A., *Langmuir* **4,** 945 (1988).
21. Martinez, R., and Barteau, M. A., *Langmuir* **1,** 684 (1985).
22. Kim, K. S., and Barteau, M. A., *Surf. Sci.* **223,** 13 (1989).
23. Hoflund, G. B., Yin, H.-L., Grogan, A. L., Jr., Asbury, D. A., Yoneyama, H., Ikeda, O., and Tamura, H., *Langmuir* **4,** 346 (1988) and references therein.
24. Kim, K. S., Barteau, M. A., and Farneth, W. E., *Langmuir* **4,** 533 (1988).
25. Ko, E. I., Benziger, J. B., and Madix, R. J., *J. Catal.* **62,** 264 (1980).
26. Davis, J. L., and Barteau, M. A., *Langmuir* **5,** 1299 (1989).
27. Kim, K. S., PhD dissertation, University of Delaware, Newark, DE, 1988.
28. McKay, J. M., and Henrich, V. E., *Surf. Sci.* **137,** 463 (1984).
29. Firment, L. E., *Surf. Sci.* **116,** 205 (1982).
30. Kurtz, R. L., *Surf. Sci.* **177,** 526 (1986).
31. Lui, K., Vest, M., Berlowitz, P., Akhter, S., and Kung, H. H., *J. Phys. Chem.* **90,** 3138 (1986).
32. Tanaka, K., Miyahara, K., and Toyoshima, I., *J. Phys. Chem.* **88,** 3504 (1984).
33. Gelius, U., Heden, P. F., Hedman, J., Lindberg, B. J., Manne, R., Nordberg, R., Nordling, C., and Siegbahn, K., *Phys. Scr.* **2,** 70 (1970).
34. Kishi, K., and Ikeda, S., *Appl. Surf. Sci.* **5,** 7 (1980).
35. Onishi, H., Aruga, T., Egawa, C., and Iwasawa, Y., *Surf. Sci.* **193,** 33 (1988).
36. Bowker, M., and Madix, R. J., *Appl. Surf. Sci.* **8,** 299 (1981).
37. Bowker, M., *Vacuum* **33,** 669 (1983).
38. Barteau, M. A., and Madix, R. J., *J. Electron Spectrosc. Relat. Phenom.* **31,** 101 (1983).
39. Sabattini, L., Morelli, B., Zambonin, P., and DeAngelis, B. A., *J. Chem. Soc. Faraday Trans.* **75,** 2628 (1979).
40. Schiess, P., and Radimerski, P., *Helv. Chim. Acta* **57,** 2583 (1974).
41. Bock, H., Mohmand, S., Hirabayashi, T., and Semkow, A., *Chem. Ber.* **115,** 1339 (1982).
42. Root, T. W., and Duncan, T. M., *J. Catal.* **101,** 527 (1986).
43. Zecchina, A., Coluccia, S., and Morterra, C., *Appl. Spectrosc. Rev.* **21,** 259 (1985).
44. Peng, X. D., PhD dissertation, University of Delaware, Newark, DE 1988.
45. Gonzalez, F., Munuera, G., and Prieto, J. A., *J. Chem. Soc. Faraday Trans.* **74,** 1517 (1978).
46. Gates, B.C., Katzer, J. R., and Schuit, G. C. A., "Chemistry of Catalytic Processes." McGraw–Hill, New York, 1979.
47. Carrizosa, I., and Munuera, G., *J. Catal.* **49,** 174 (1977).
48. Boonstra, A. H., and Mutsaers, C. A. H. A., *J. Phys. Chem.* **79,** 2025 (1975).
49. Rives-Arnau, V., and Sheppard, N., *J. Chem. Soc. Faraday Trans.* **76,** 394 (1980).
50. Rives-Arnau, V., and Sheppard, N., *J. Chem. Soc. Faraday Trans.* **77,** 953 (1981).
51. Halliday, M. M., Kemball, C., and Leach, H. F., *J. Chem. Soc. Faraday Trans.* **70,** 1743 (1974).
52. Cotton, F. A., and Wilkinson, G., "Advanced Inorganic Chemistry," 4th ed. Wiley, New York, 1980.